Solid Freeform Fabrication 2016: Proceedings of the 27th Annual International Solid Freeform Fabrication Symposium – An Additive Manufacturing Conference
Reviewed Paper

Optimization of Low One-photon Polymerization for Hydrostatic 3D Printing of Silicone Material

Dong Sung (Danny) Kim[1], Steven Thompson[1], Melissa Grunlan[2], Bruce L. Tai[1]

[1]Department of Mechanical Engineering, Texas A&M University, College Station, 77843
[2]Department of Biomedical Engineering, Texas A&M University, College Station, 77843

Keywords: additive manufacturing; silicone printing; low one-photon polymerization

Abstract

This study investigated the parameter optimization of low one-photon polymerization in hydrostatic 3D printing (H3P). H3P produces 3D structures in a hydrostatic condition with minimum or no physical supports, used particularly for soft materials that typically require substantial supports to hold the position and shape in conventional 3D printing methods. H3P allows for "in-liquid" polymerization to happen by low one-photon polymerization (LOPP) to cure the silicone at the focusing spot inside of the resin. With the selected UV-curable silicone, different wavelengths, light intensities, and exposure times were investigated to achieve an ideal LOPP. The ideal LOPP should have a wide time window to precisely control the polymerization size and produce a consistent geometry. This is largely dependent on the light wavelength and then the intensity. In this study, the wavelength of 387 nm with the absorbance rate of 0.008 was found the optimal setting for the selected silicone among 365 nm (0.051 absorbance rate) and 405 nm (nearly 0 absorbance rate) wavelengths. The results showed that the parameters for LOPP are very selective.

Introduction

Additive manufacturing (also known as 3D printing) is an emerging technology to enable various materials to be fabricated with three-dimensional geometries. The source materials such as metals, ceramics and plastics are generally stiff and rigid. Soft materials such as silicones and gelatins are even more challenging to print. If it becomes possible to print with the soft materials, its applications could be expanded to medical simulators [1], tissue engineering [2], soft robotics [3], and so on. The main issues present with the soft materials are related to their low shape stability [4]. Due to their low stiffness and the effect of gravity, the structures could easily collapse or deform during, or even after the printing. Molding technique is a common fabrication process for the soft materials [5]; however, its limitations compared to additive manufacturing are its difficulties in making structures with complex and enclosed geometries [6-8].

Support structures are commonly used to improve the shape stability in the 3D printing process. Depending on a specimen's geometry, even rigid materials may need to be printed with support structures [9]. With regards to the soft materials, a substantial amount of support structures are required to enhance the specimen's stability during printing. This approach results in both a huge waste of material and time during printing and post-processing. In spite of the considerable support structures, the structures can still be easily deformed due to their low stiffness and the effect of gravity.

In previous research [10], a hydrostatic 3D printing method was introduced to overcome the issues with soft material printing. H3P is an in-liquid process to create an immersed part in a hydrostatic condition as a result of a similar density. Hence, hydrostatic forces could support the structure and its shape with minimum or no physical support structures mentioned before. To achieve this in-liquid process, the H3P utilizes one of direct writing techniques known as low one-photon polymerization (LOPP) [11]. Theoretically, the LOPP could cure any point inside the liquid resin because the polymerization region is limited only to the focusing spot. On the other hand, conventional processes such as stereolithography (SLA) utilize regular one-photon polymerization (OPP). OPP cures the material along the whole beam path. Therefore, SLA is a surface lithography method to build a 3D structure from sliced 2D images, as opposed to H3P to directly draw 3D structure inside of the resin.

There are two critical requirements to successfully initiate the LOPP. The first requirement is to find a wavelength with a low absorbance rate. Each photopolymer has a different absorbance rate that depends on the selected wavelength. LOPP utilizes a wavelength with a low absorbance rate to induce polymerization at the focal spot. The second requirement is to create a wide beam gradient to maximize the effect of the low absorbance rate of the chosen wavelength. The beam gradient represents the photon distribution of the beam. Generally, the beam gradient is decided by the property of the final lens, called numerical aperture (N.A.). The number of the numerical aperture represents the beam shape. As the number increases, the beam shape becomes a shorter conical shape and becomes wider. This causes a trade-off between the numerical aperture and the focal length. In air, the maximum number of the N.A. is 1.

From previous research, it was found that the main parameters of LOPP for H3P are wavelength, intensity and exposure time [10]. Wavelength is the most critical factor to determine whether LOPP is possible in the photopolymer. Intensity, along with exposure time, control the level of LOPP; high intensity and long exposure time can still transform LOPP into an OPP effect. The optimal settings to control LOPP are still unclear. To continue the research on the subject, this study investigated the LOPP phenomena by changing the combinations of the three parameters. The next section summarizes the materials and methods used in the study, followed by the experimental results. Discussion will be present afterward to comment on the use of LOPP in hydrostatic 3D printing.

Materials and Methods

In this study, a non-commercial silicone photopolymer provided by Dow-Corning (Midland, MI) was used for the experiments. It is a two-part material; one part is a silicone resin, and the other part is a photoinitiator. Figure 1 on the next page shows the absorbance spectrum of the photoinitiator measured by a U-4100 Hitachi spectrophotometer (Tokyo, Japan). The absorbance rates become less than 0.1 after a wavelength of 350 nm, becoming less than 0.1 thereafter. To realize the LOPP effect, three wavelengths were selected based on the absorbance rates and the availability and practicality of locating optical parts. The first wavelength selected was 365 nm with an absorbance rate of 0.051. The second wavelength selected was 387 nm with an absorbance rate of 0.008. The third wavelength selected was 405 nm with an absorbance rate nearly zero.

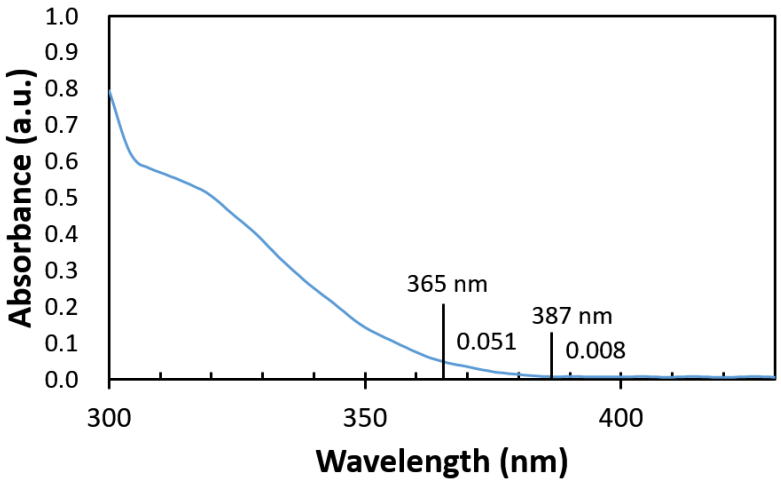

Figure 1: Absorption spectrum of the material

The lamp system has a beam spectrum from 250 nm to 650 nm. The beam from the lamp system is guided to the optical lens array by a light guide. Figure 2(b) shows the details of the lens array provided by Edmund Optics Incorporated (Barrington, NJ, USA). The lens array consists of a guide holder, two iris diaphragms, a collimating lens, a band pass filter, and a focusing lens. The guide holder fixes the optical cable to the array and the collimating lens creates a uniform and parallel beam with the beam from the optical cable. The beam goes through the band pass filter which adjusts the incoming beam to a specific wavelength on exit among the wide beam spectrum.

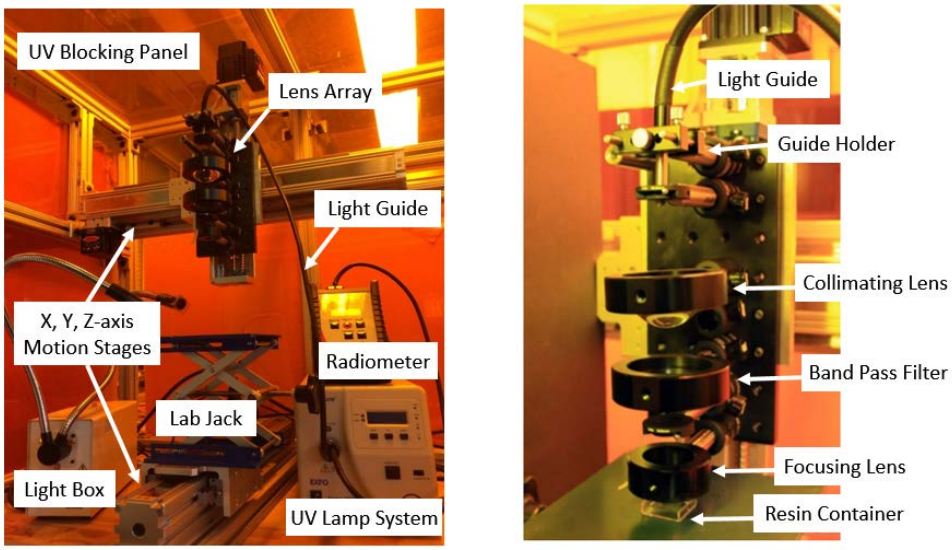

(a) (b)

Figure 2: Experimental setup: (a) an overview and (b) details for the optical lens array

In this experiment, three different band pass filters were used to obtain the 365 nm, the 387 nm, and the 405 nm wavelengths. The final lens focuses the beam from the band pass filter with the back focal length (BFL) equal to 6.9 mm. The final lens has a numerical aperture of 1 to produce the largest possible beam gradient in the air. The combination of the collimating lens and

the focusing lens produces a magnification of 0.2 which creates a focal spot with a 1 mm diameter. The iris diaphragms were used to align the beam and the beam intensity is adjusted by the electrical iris shutter of the lamp system. The opening level can be controlled from 1% to 100% and the radiometer was used to get actual beam powers of the each intensity. A small acrylic box with the external dimensions of 25.4 mm by 25.4 mm by 6.3 mm was used as a resin container.

The experimental method was designed to quantitatively measure the LOPP effects under a stationary condition called a single-spot test. Figure 3(a) illustrates this single-spot test. The resin container is filled with the silicone liquid resin. The focused beam generates pillars of different heights depending on the chosen parameters of wavelength, intensity, and exposure time. The reason that the focal point of the beam is set near the bottom is to enable the cured silicone pillars to remain standing after the test for the measurement purpose. OPP and LOPP-produced pillars were distinguished by the height relative to the resin depth. The first pillar in Figure 3(a) is a 4.8 mm, full-height pillar equal to the resin depth. This means the resin was cured along the whole beam path. Therefore, the full-height pillar represents that the parameters initiated the regular one-photon polymerization (OPP). The second pillars grew upwards from the bottom surface to the certain points inside the resin. The partial-height pillars exemplifies that the resin was cured only near the focal point. Therefore, the partial-height pillar indicates the parameters initiated low one-photon polymerization (LOPP). In the experiment, the 4 by 4 array shown in the Figure 3(b) was used to get 16 testing points with an incremental exposure time for each resin container. Each point was spaced 5 mm apart from each other.

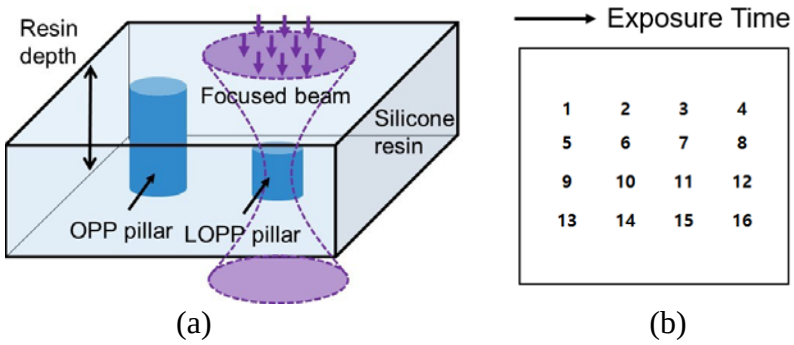

Figure 3: (a) Schematic diagram of the single-spot test and (b) the 4 by 4 testing array with incremental exposure time

Experimental Results

The experiment was conducted by changing the parameters of wavelength, intensity, exposure time. The selected wavelengths were 365 nm, 387 nm and 405 nm. The intensities selected were 100%, 70%, 50%, and 30%. This was originally a 3 by 4 design of experiment (DOE). With the 365 nm wavelength, all intensities listed were tested. However, with the 387 nm wavelength, only the intensity of 100% was tested since a lower intensity was unable to generate visible pillars. Similar with 405 nm, even 100% intensity could not produce any visible parts due to the ultra-low absorbance rate. As a result, there were four testing results for 365 nm and one for 387 nm wavelength.

The exposure time was from 30 seconds to 180 seconds, recording data every at every 10

second interval for the 365 nm wavelength. The exposure time was from 30 seconds to 330 seconds, recording data every at every 10 second interval for the 387 nm wavelength. A longer exposure time used in 387 nm was because of a lower absorbance rate. Figure 4 and Figure 5 show the physical samples with 365 nm and 387 nm wavelengths. To obtain the pillar dimensions, the samples were coated with powder and measured by an Alicona Model G4 surface profiler (Graz, Austria). Figure 6 shows one of the 3D models generated by the profiler.

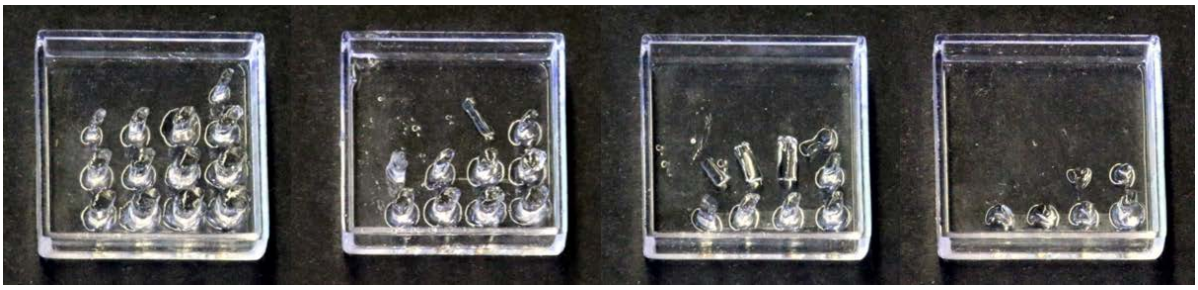

(a) (b) (c) (d)

Figure 4: Physical sample**s** with 365 nm wavelength and exposure time 30 seconds to 180 seconds at the intensities of (a) 100 % (b) 70 % (c) 50 % and (d) 30 %

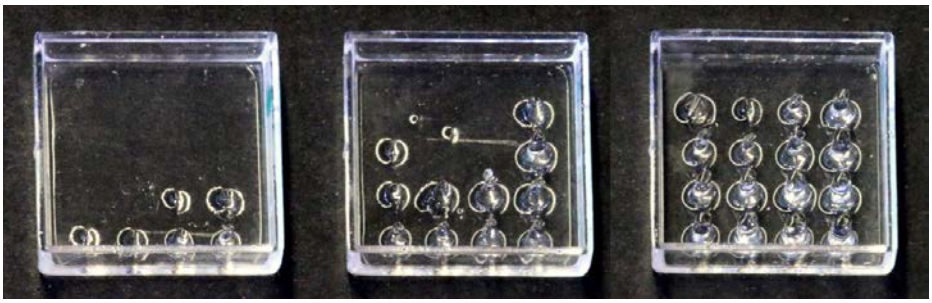

(a) (b) (c)

Figure 5: Physical samples with 387 nm wavelength at 100% intensities for exposure time of (a) 30 seconds to 180 seconds, (b) 100 seconds to 250 seconds, and (c) 180 seconds to 330 seconds

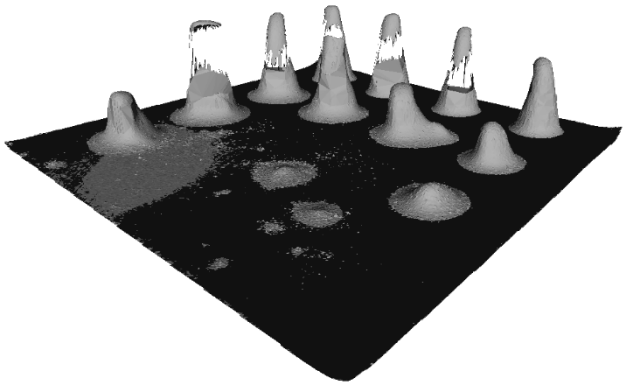

Figure 6: 3D model generated by the surface profiler
(387 nm wavelength, 100 % intensity and exposure time 100 seconds to 250 seconds)

The results with the 365 nm wavelength are shown in Figure 7. With 100% intensity, no pillars are present up until 50 seconds. After 60 seconds, the full-height pillars were found to display the OPP effect. With 70% intensity, no pillars are present up until 80 seconds. At 90 seconds, the pillar was partially cured with a height 2.5 mm but collapsed and stretched prior to the measurement. At 100 seconds and 110 seconds, partial-height pillars were observed with the heights of 2.9 mm and 4.7 mm respectively. This means a gap between the top surface of the pillars and the resin surface during 90 to 110 second exposure time, which verifiably displays the LOPP effect. The pillars between 120 seconds and 180 seconds have the full-height of 4.8 mm, displaying the OPP effect. With 50% intensity, no pillars are present up until 90 seconds. Between 100 seconds and 120 seconds, the partial pillars were found with the heights of 2.1 mm, 3.7 mm and 4.6 mm respectively, displaying the LOPP effect.

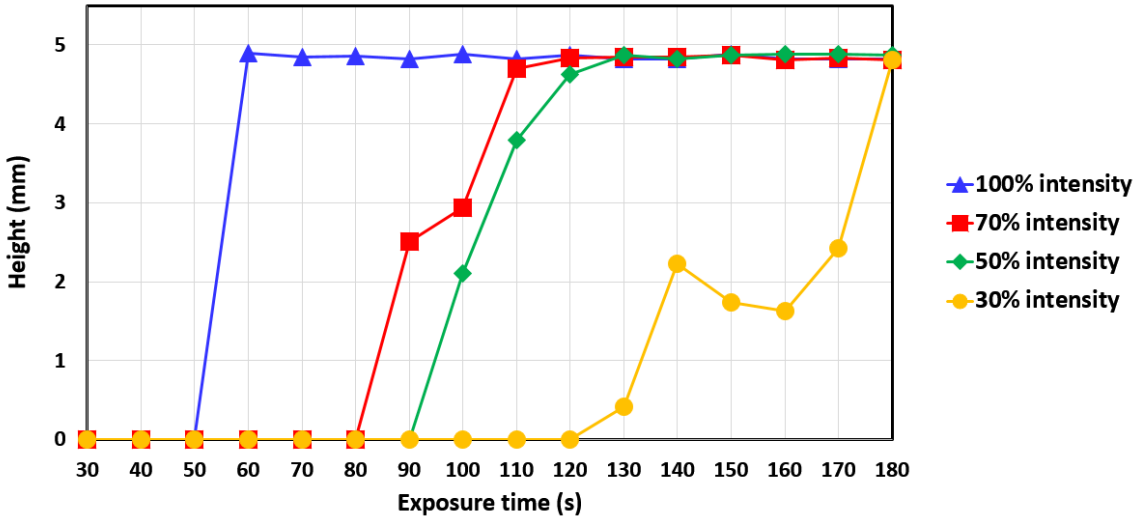

Figure 7: Results of the 365 nm wavelength test, displaying pillar height vs. exposure time with 100%, 70%, 50% and 30% intensities

After 130 seconds, the pillars were fully cured with the height of 4.8 mm, displaying the OPP effect. The pillars between 100 seconds and 130 seconds collapsed before proper measurements could be taken. With 30% intensity, no pillars are present up until 120 seconds. Between 130 seconds and 170 seconds, the partial pillars were observed with the heights of 0.4 mm, 2.2 mm, 1.7 mm, 1.6 mm and 2.4 mm respectively, displaying the LOPP effect. At 180 seconds, the full-height pillar was found, displaying the OPP effect.

Figure 8 shows the results of the 387 nm wavelength test with 100% intensity. No figure with 70% intensity will be presented, as no pillars were found within the defined exposure time. For the 387 nm wavelength, the exposure time was extended to 330 seconds. With 100% intensity, there were no pillars present up until 120 seconds. Between 130 seconds and 200 seconds, the partial pillars were found with the heights of 0.6 mm, 0.9 mm, 0.7 mm, 1.4 mm, 2.0 mm, 1.9 mm, 2.6 mm, 4.4 mm respectively, displaying the LOPP effect. After 210 seconds, the full pillars were observed with the height of 4.8 mm, displaying the OPP effect.

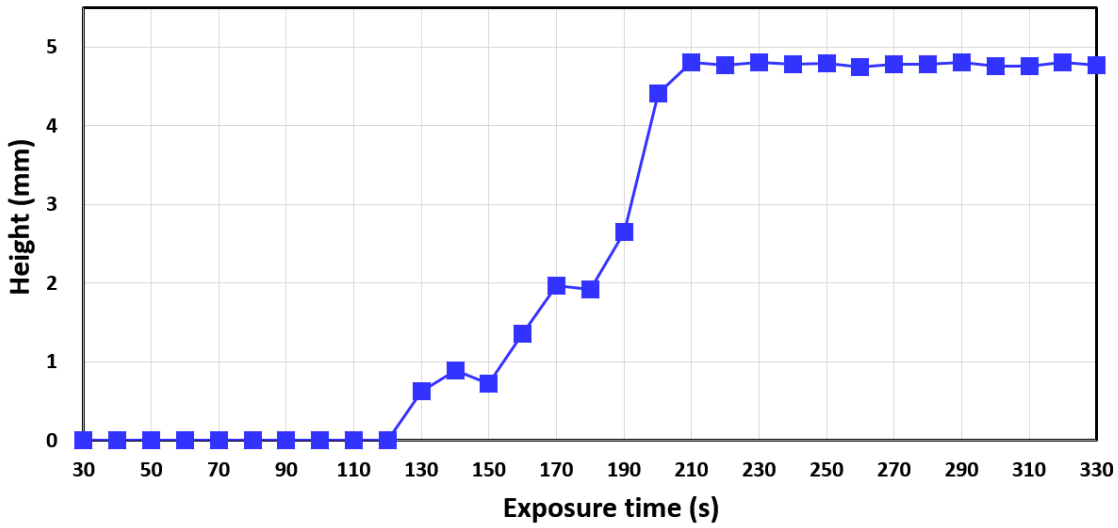

Figure 8: Results of the 387 nm wavelength test, displaying pillar height vs. exposure time with 100% intensity

Discussion

Using the parameters of wavelengths, intensities and exposure times, OPP and LOPP effects were successfully observed. Especially due to the different absorbance rates related to the wavelengths, different polymerization trends were observed.

For the 365 nm wavelength with an absorbance rate of 0.051, the 100% intensity showed only the OPP effect, which was observed by the full-height pillars. The intensities of 70%, 50% and 30% initiated both OPP and LOPP effects depending on the exposure times. As the intensity becomes lower, more partial-pillars were observed with longer exposure times as shown in Figure 7. This leads us to believe that the intensity can control the time window for the LOPP effect. Even though the lower intensities require longer exposure time to cure the pillars, the lower intensities can achieve much smaller pillar sizes in the LOPP effect. This leads us to believe that better resolutions could be achieved through lower intensities. However with the 30% intensity, the pillar growth was not stable between 140 second and 170 seconds. This might be due to the low stability of the lamp system under a low power output.

For the 387 nm wavelength with an absorbance rate 0.008, the 100% intensity cured the pillars, yet the 70% intensity could not produce any pillars. Figure 8 shows that the partial-height pillars existed between 130 seconds and 200 seconds. Compared to the results with the 365 nm wavelength and 30% intensity, the 387 nm wavelength has a wider time window for the LOPP effect as shown in Figure 9. Even though the first pillars were found at the same exposure time of 130 seconds, the 387 nm wavelength has more stable and wider time window for the LOPP effect between 130 seconds and 200 seconds, compared to the results with the 365 nm wavelength. This leads us to believe that the 387 nm wavelength can provide more reliable and precise controls to the polymerization process. Figure 10 shows the pillar volume vs. exposure time with the 365 nm and the 387 nm wavelength. To better understand the growth trends, the pillar volumes with the two wavelengths were compared. The diameters of the pillars were not directly compared due to the difficulty of judging the diameters of non-cylindrical pillar shapes. With the LOPP effect, the

volume increased relatively smoothly. However, for the 365 nm wavelength, the pillar volume at the 180 seconds mark rapidly increased due to the sudden radial growth of the pillar. This is because the pillar was ultimately made by the OPP effect and not by the LOPP effect. The 387 nm wavelength shows the relatively slow growth, even for the pillar at the 210 second mark made by the OPP effect. The slow growth rate is primarily due to the low absorbance rate.

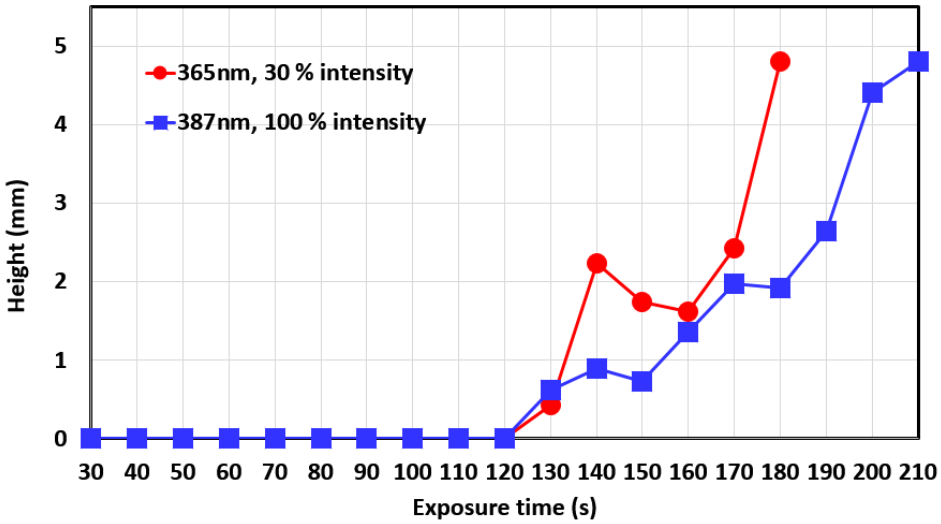

Figure 9: Pillar height vs. exposure time, both for the 365 nm wavelength and 30% intensity and for the 387 nm wavelength and 100% intensity

For the 387 nm wavelength, no collapsed pillars were present as compared to the results of the 365 nm wavelength. This is due primarily to the pillars with the short exposure times of the 387 nm wavelength having shorter heights and smaller volumes than the ones with the 365 nm wavelength. Therefore, the short and thin pillars stand on the bottom without collapse. The 365 nm wavelength and the 387 wavelength have different pillar shapes as shown in Figure 11.

The pillars with the 365 nm wavelength for all intensities tested except for the intensity 30% have cylindrical shapes as shown in Figure 11(a). In contrast, all pillars with the 387 nm wavelength have tapered-cylindrical shapes as shown in Figure 11(b). This shape difference results from the different effective areas due to the different absorbance rates, along with a wide beam gradient and a non-uniform distributed light intensity across the beam path. There is highly non-linear polymerization occurring among different wavelengths, different intensities, and even within the focusing spot. Further work on this topic would be building an optics model based on the material absorbance rate.

The smallest pillar size achievable can be seen as a voxel, a basic unit in constructing 3D images. Smaller voxels lead to better resolution, whereas larger voxels lead to increased productivity. In this particular material, 387 nm with 100% light intensity provides a good comprise between these two options. An estimated voxel size is close to 0.5 mm based on Figures 9 and 10. The voxel shape might be close to an ellipsoid rather than sphere or cube; however the exact shape is undetermined due to the pillars attaching on the bottom surface.

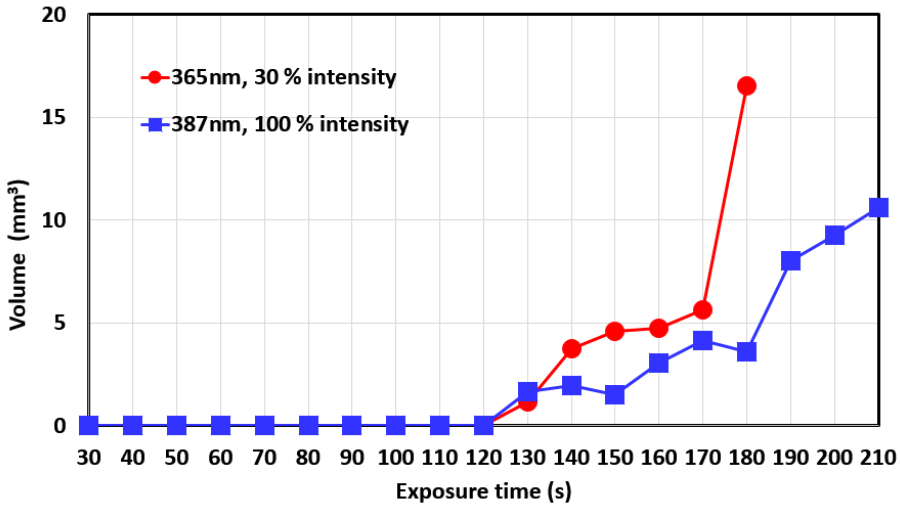

Figure 10: Pillar volume vs. exposure time, both for the 365 nm wavelength and 30% intensity and for the 387 nm wavelength and 100% intensity

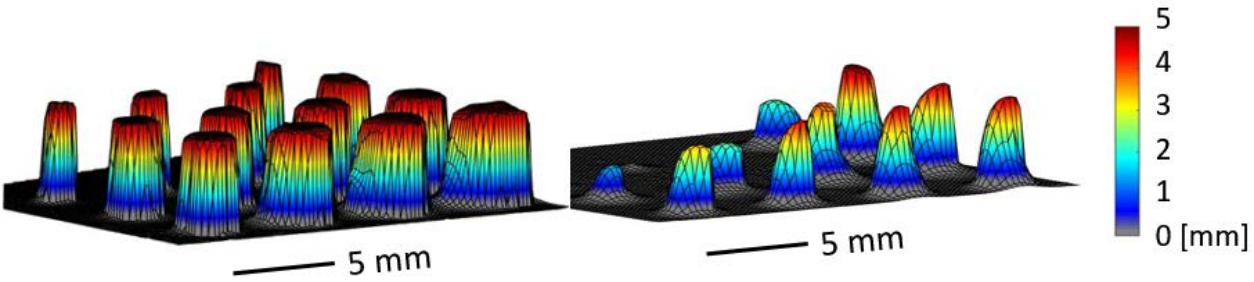

(a) (b)

Figure 11: The shapes of the pillar with different wavelengths, (a) cylindrical shapes with the 365 nm wavelength, (b) tapered-cylindrical shapes with the 387 nm wavelength

Conclusions

This study investigated the parameter optimization of low one-photon polymerization in hydrostatic 3D printing (H3P). Although the parameters were specific to the selected material, the results have demonstrated the feasibility to control the in-liquid LOPP. It was determined that the three main parameters that should be adjusted to achieve a reliable LOPP effect were wavelength, intensity and exposure time. The wavelength was observed to define the time window for the LOPP effect. A wavelength with a lower absorbance rate (387 nm in this study) provided a more stable and wider window to achieve better resolutions with controllable polymerization. However, the wavelengths with an extremely low absorbance rate (405 nm in this study) could not initiate any polymerization. The intensity can also control the window with the limitation that lower intensities could cause an unstable LOPP effect. Low intensities were more easily inconsistent due to the small power output of the optical system; therefore, relatively higher intensities could lead to a more stable LOPP effect. Lastly, the exposure time was observed to control the total energy absorbance. Long exposure times resulted in the OPP effect due to excessive energy absorbance. The exposure time is directly related to the feed rate selection in a printing scenario. Thus, the

printing resolution or voxel size can be altered during the process depending on the geometric features, in an effort to maximize the printing efficiency. In conclusion, the optimization of low one-photon polymerization can be actualized with the ideal combination of a selected wavelength with a relatively low absorbance rate, relatively strong intensity, combined with a stable power output and short exposure times. The future work will be focused on a moving condition of the LOPP to realize H3P.

Acknowledgements

This research is partially supported by Los Alamos National Labs and National Science Foundation Grant (#1522877). The authors would also like to acknowledge the material supports from Dr. Rocky Zhu of Dow Corning Corporation (Midland, MI). The authors would also like to thank Zhujian Feng and Jigar Patel for the technical supports of the Alicona G4 machine.

References

[1] Laurent, M., Scheer, P., Dejou, J., and Laborde, G., 2008, "Clinical evaluation of the marginal fit of cast crowns – validation of the silicone replica method," Journal of Oral Rehabilitation, 35(2), pp. 116-122.

[2] Place, E. S., George, J. H., Williams, C. K., and Stevens, M. M., 2009, "Synthetic polymer scaffolds for tissue engineering," Chemical Society Reviews, 38(4), pp. 1139-1151.

[3] Roche, E. T., Wohlfarth, R., Overvelde, J. T. B., Vasilyev, N. V., Pigula, F. A., Mooney, D. J., Bertoldi, K., and Walsh, C. J., 2014, "A Bioinspired Soft Actuated Material," Advanced Materials, 26(8), pp. 1200-1206.

[4] Muroi, H., Hidema, R., Gong, J., and Furukawa, H., 2013, "Development of Optical 3D Gel Printer for Fabricating Free-Form Soft & Wet Industrial Materials and Evaluation of Printed Double-Network Gels," Journal of Solid Mechanics and Materials Engineering, 7(2), pp. 163-168.

[5] Kang, H.-W., and Cho, D.-W., 2012, "Development of an Indirect Stereolithography Technology for Scaffold Fabrication with a Wide Range of Biomaterial Selectivity," Tissue Engineering. Part C, Methods, 18(9), pp. 719-729.

[6] Park, J.-H., Choi, S.-O., Kamath, R., Yoon, Y.-K., Allen, M. G., and Prausnitz, M. R., 2007, "Polymer particle-based micromolding to fabricate novel microstructures," Biomedical Microdevices, 9(2), pp. 223-234.

[7] Lord, H. A., and Williams, G., 1975, "Mold-filling studies for the injection molding of thermoplastic materials. Part II: The transient flow of plastic materials in the cavities of injection-molding dies," Polymer Engineering & Science, 15(8), pp. 569-582.

[8] Rosof, B. H., 1989, "The metal injection molding process comes of age," The Journal of The Minerals, Metals & Materials Society, 41(8), pp. 13-16.

[9] Hu, K., Jin, S., and Wang, C. C. L., 2015, "Support slimming for single material based additive manufacturing," Computer-Aided Design, 65, pp. 1-10.

[10] Kim, D. S., and Tai, B. L., 2016, "Hydrostatic support-free fabrication of three-dimensional soft structures," Journal of Manufacturing Processes.

[11] Li, Q., Do, M. T., Ledoux-Rak, I., and Lai, N. D., 2013, "Concept for three-dimensional optical addressing by ultralow one-photon absorption method," Optics Letters, 38(22), pp. 4640-4643.